

Article

Porphyrin Hetero-Trimer Involving a Hydrophilic and a Hydrophobic Structure with Application in the Fluorescent Detection of Toluidine Blue

Anca Lascu ^{1,*}, Camelia Epuran ¹, Ion Fratilescu ¹, Mihaela Birdeanu ² , Liliana Halip ¹ and Eugenia Fagadar-Cosma ^{1,*} 

¹ Institute of Chemistry “Coriolan Dragulescu”, Mihai Viteazu Ave. 24, 300223 Timisoara, Romania

² National Institute for Research and Development in Electrochemistry and Condensed Matter, Plautius Andronescu Street 1, 300224 Timisoara, Romania

* Correspondence: alascu@acad-icht.tm.edu.ro (A.L.); efagadar@yahoo.com (E.F.-C.)

Abstract: The combination of a metallated porphyrin, Pt(II)-5,10,15,20-tetrakis-(4-allyloxyphenyl)-porphyrin (Pt-allyloxyPP), and a water-soluble porphyrin, 5,10,15,20-tetrakis(4-sulfonatophenyl)-porphyrin (TSPP), leads to the formation of a porphyrin hetero-trimer. The hetero-trimer, consisting of two TSPP molecules linked via oxygen atoms axially to the platinum atom in the Pt-allyloxyPP molecule, was characterized by UV–Vis, FT-IR, fluorescence, and ¹H-NMR spectroscopy, and the proposed structure was confirmed. The new porphyrin hetero-trimer offers both the advantage of enhanced fluorescence and the presence of multiple sites for the detection of toluidine blue, due to its high affinity for acidic binding sites. This work brings attention to the purposely designed fluorescent sensor for toluidine blue, in the biologically relevant concentration domain of 1.9×10^{-6} – 6.39×10^{-5} M, with a very good accuracy.

Keywords: platinum-porphyrin; tetra-sulfonatophenyl-porphyrin; porphyrin trimer; fluorescence detection; toluidine blue



Citation: Lascu, A.; Epuran, C.; Fratilescu, I.; Birdeanu, M.; Halip, L.; Fagadar-Cosma, E. Porphyrin Hetero-Trimer Involving a Hydrophilic and a Hydrophobic Structure with Application in the Fluorescent Detection of Toluidine Blue. *Chemosensors* **2022**, *10*, 481. <https://doi.org/10.3390/chemosensors10110481>

Academic Editor: Xiaobing Zhang

Received: 6 October 2022

Accepted: 9 November 2022

Published: 15 November 2022

Publisher’s Note: MDPI stays neutral with regard to jurisdictional claims in published maps and institutional affiliations.



Copyright: © 2022 by the authors. Licensee MDPI, Basel, Switzerland. This article is an open access article distributed under the terms and conditions of the Creative Commons Attribution (CC BY) license (<https://creativecommons.org/licenses/by/4.0/>).

1. Introduction

Supramolecular systems based on porphyrins and their dimers are the subject of ongoing research topics and have found their application as antennas [1,2] in medicinal [3] and detection fields [4–6].

The porphyrin dimers and trimers can be formed either by combining two or three porphyrin molecules, having the same or different structures, together or by bridging the moieties via linkers. Examples of porphyrin homo- and hetero-dimers and trimers and their various applications are presented in Table S1 in the Supplementary Materials [1–3,5,7–19].

Toluidine blue (TB), with IUPAC name (7-amino-8-methylphenothiazin-3-ylidene)-dimethylammonium chloride (Figure 1), is a dye commonly used for the staining of DNA and RNA, as it possesses a high affinity for acidic compounds [20].

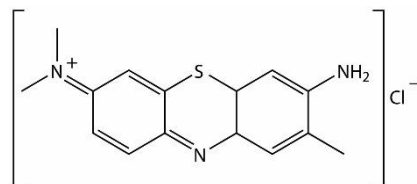


Figure 1. Structure of toluidine blue (TB).

TB is employed in the minimally invasive chemiluminescence diagnosis of oral cancer [21,22], in the quantification of mast cells in skin images [23], and as dye in peripheral

nerve axonal histomorphometry in light micrographs [24]. The *in vitro* evaluation of toluidine blue in the Ames test (a biological assay to test whether a certain chemical induces DNA mutations and is, therefore, carcinogenic) show that 50 μg TB/plate have clastogenic and mutagenic effects [25,26]. In concentrations >50 μM , TB significantly decreased the mitochondrial membrane potential and increased the reactive oxygen species production after 4 h *in vitro* exposure of human lung adenocarcinoma cells (A549) [27]. That is the reason why the monitoring of the toluidine blue is a demand, in order to prevent overcoming of safety doses during imaging tests.

There are few reports in the literature regarding the detection or removal of TB, with one of them mentioning its removal from wastewaters using remnant black tea leaves [28]. It was concluded that 150 μm diameter particles of black tea leaves remnants could adsorb 50 mg/g of TB.

The original aspect of this work consists of the first-time development of a toluidine blue fluorescence sensor. The formation of a novel porphyrin hetero-trimer, created by the direct combination of a metalloporphyrin, Pt(II)-5,10,15,20-tetrakis-(4-allyloxyphenyl)-porphyrin (Pt-allyloxyPP) (Figure 2a), and a water-soluble porphyrin, 5,10,15,20-tetrakis(4-sulfonatophenyl)-porphyrin (TSPP) (Figure 2b), is capable of fluorescently detecting toluidine blue with high accuracy. The new hetero-trimer (Figure 2c) offers both the advantage of enhanced fluorescence and the presence of multiple active sites for the linkage of toluidine blue.

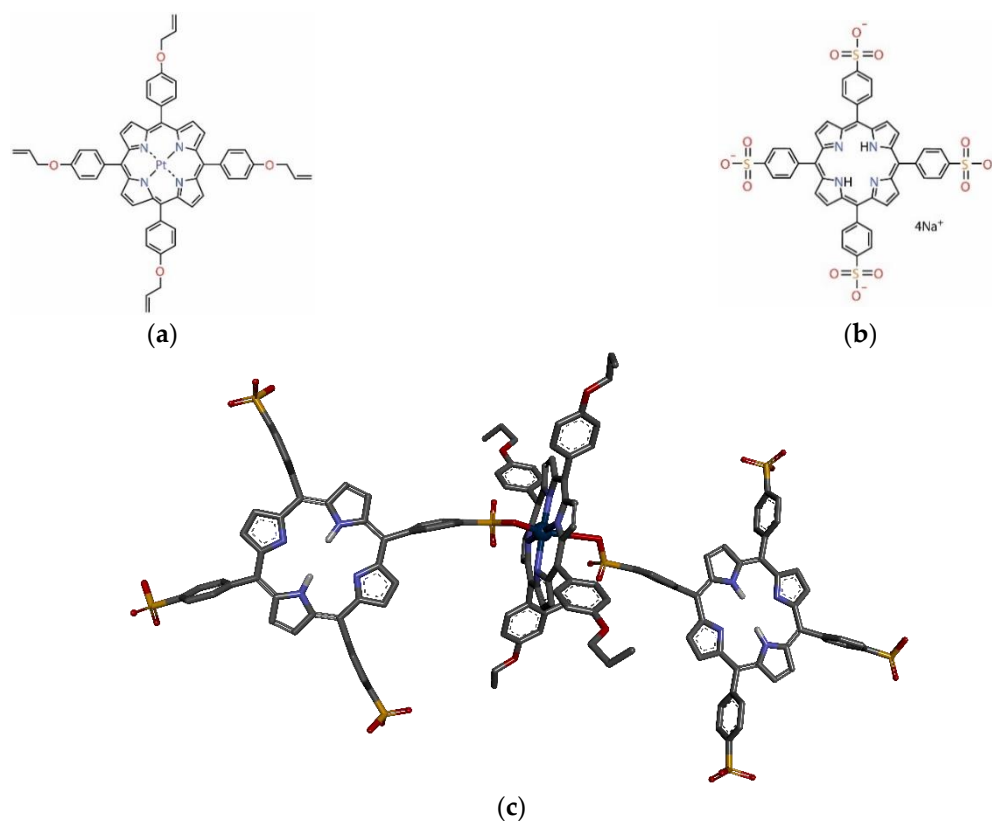


Figure 2. Chemical structures for (a) Pt(II)-5,10,15,20-tetrakis-(4-allyloxyphenyl)-porphyrin (Pt-allyloxyPP); (b) 5,10,15,20-tetrakis(4-sulfonatophenyl)-porphyrin (TSPP); and (c) Proposed structure of the Pt-allyloxyPP-TSPP hetero-trimer, optimized with PyMOL Molecular Graphics System. Atom color coding follows standard CPK rules: carbon-black, oxygen-red, nitrogen-blue, sulfur-yellow, platinum-dark blue, hydrogen-white.

2. Materials and Methods

2.1. Materials

The dimethyl sulfoxide was purchased from Honeywell Riedel-de Haen, Seelze Germany; toluidine blue originated from Fluka Chemika, Buchs, Switzerland; glucose (Glu), NaCl, urea, ascorbic acid (AA), and ammonium oxalate (AmOxa) from Chimreac-tiv/Reactivul (Bucuresti, Romania), sodium acetate (SA), sodium salicylate (SS), calcium gluconate (CaG), KI, and KCl from Merck, Darmstadt, Germany, and FeCl₃ from Fluka Chemie Bucks, Switzerland.

2.1.1. Obtaining of 5,10,15,20-Tetra-(4-allyloxy-phenyl)porphyrin

The free-base porphyrin was synthesized adapting the Lindsey method, by condensation of 4-allyloxybenzaldehyde with pyrrole in propionic acid or by functionalization of *meso*-5,10,15,20-tetra-(4-hydroxyphenyl)porphyrin, with bromopropylene in the presence of anhydrous potassium carbonate, as mentioned in earlier reports [29].

2.1.2. Obtaining of Pt(II)-5,10,15,20-Tetra-(4-allyloxy-phenyl)porphyrin

The synthesis of Pt-allyloxyPP was achieved by metalation of the porphyrin-base, 5,10,15,20-tetra-(4-allyloxy-phenyl)porphyrin with bis(benzonitrile)platinum(II) chloride, and sodium acetate in chlorobenzene, as we previously published [30].

2.1.3. Obtaining of Benzenesulfonic Acid, 4,4',4'',4'''-(21H,23H-Porphine-5,10,15,20-tetra-yl) tetrakis-tetrasodium Salt, Commonly Named as 5,10,15,20-Tetrakis(4-sulfonatophenyl)-porphyrin (TSPP)

TSPP was obtained using methods reported in the literature [31–34] by treating *meso*-tetrakis-phenylporphyrin with oleum sulfuric acid and raising the temperature up to 80 °C. This temperature was maintained at least 40 min under intense stirring. After cooling the reaction mixture to room temperature and careful treatment with distilled water, the green reaction mass was neutralized with sodium hydroxide (*c* = 2 M) when the solution turned purple. Evaporation of the water and drying under vacuum were the next steps. The UV-Vis, fluorescence, and FT-IR spectra of the TSPP are presented in Supplementary File, Figures S1–S4 [34–41].

2.2. Apparatus

UV-Vis spectra were obtained with a JASCO spectrophotometer (Pfungstadt, Germany), model V-650, using quartz cuvettes with a radiation passage length of 1 cm. An 80 MHz high-performance nuclear magnetic resonance benchtop spectrometer, model Fourier 80 (Wissembourg, France), was used to record ¹H-NMR spectra. AFM images were taken with a Nanosurf[®] EasyScan 2 Advanced Research AFM microscope device (Liestal, Switzerland), from samples casted on pure silica plates. The infrared spectra were obtained with a Jasco spectrometer (Hachoji, Tokyo, Japan), model FT/IR-4200 Type A, in KBr pellets.

The proposed structure for the trimer complex was optimized with the program Py-MOLMolecular Graphics System, Version 1.7.4 Schrödinger (LLC New York, NY, USA, 2015).

The emission spectra were recorded for the DMSO/water solution at room temperature (25 ± 2 °C) in the 500–800 nm wavelength domain, with excitation wavelength of 419 nm, an excitation slit of 10 nm, emission slit of 5 nm, and no filter. The scanning rate was 100 nm/min on a Perkin-Elmer apparatus (PerkinElmer, Inc./UK Model/LS 55, Waltham, MA, USA), model LS 55.

2.3. Formation of the Pt-allyloxyPP-TSPP Hetero-Trimer

To Pt-allyloxyPP solution in DMSO (5 mL; *c* = 9.167 × 10^{−5} M), small volumes (varying from 0.01 mL to 0.3 mL) of TSPP acidulated solution (pH = 2.5) in water (*c* = 1.25 × 10^{−5} M), were added stepwise. Each mixture was stirred for 90 s, and the UV-Vis spectra were

recorded. The complete follow-up is presented in the Supplementary Materials (Figure S5, representing the overlapped spectra recorded during the trimer formation).

3. Results and Discussions

3.1. UV–Vis Spectroscopy

In the UV–Vis spectrum of Pt-allyloxyPP (Figure 3), all the feature characteristics for a metalloporphyrin were identified. The intense Soret band is located at 410 nm and two Q bands, representing the Q(0-1) and Q(0-0) electronic transitions, are located at 513 nm and at 596 nm, respectively.

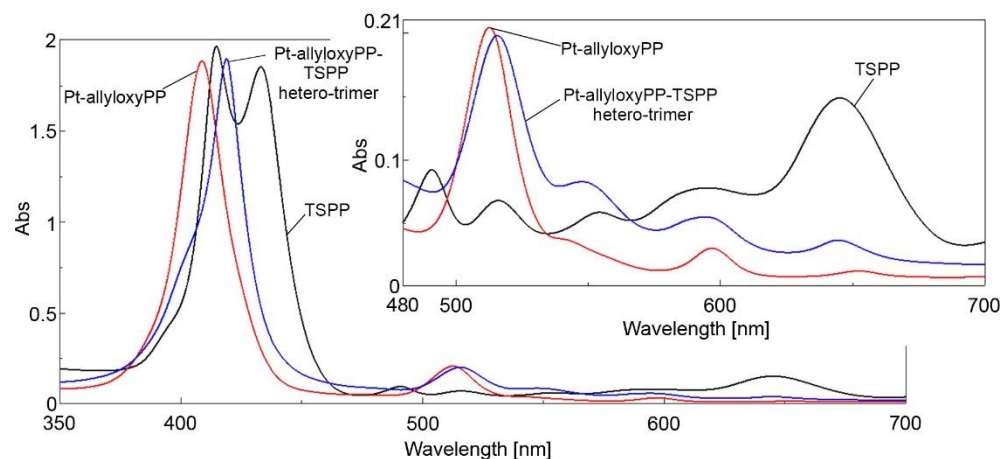


Figure 3. Overlapped UV–Vis spectra for the starting porphyrins and for the final obtained Pt-allyloxyPP-TSPP hetero-trimer.

In acid media (pH = 2), the Soret band of TSPP is split as expected, due to internal protonation [42], into two individual Lorentzian bands, one located at around 415 nm and the second around 433 nm. The increase in intensity of the Q band located at 645 nm is also a consequence of the protonation and generation of dication species [43].

The formation of the hetero-trimer is evidenced in the UV–Vis spectrum (Figure 3) by the appearance of a new Soret or B band located at a different wavelength (419 nm), as compared to the starting porphyrins (408.8 nm for Pt-allyloxyPP and 414.8 nm and 433.2 nm, respectively, due to J-type aggregates of diprotonated TSPP). In addition, a newly positioned Q band appears at 547 nm in the *etio*-type spectrum of the hetero-trimer, in which the intensities of the Q bands decrease in the following order: $Q_y(0-1) > Q_y(0-0) > Q_x(0-1) > Q_x(0-0)$.

Isosbestic points are also visible in the overlapped UV–Vis spectra recorded during the trimer formation (Figure S5 in Supplementary Files), at 414 nm and 416 nm on the Soret band and at 498 nm and 516 nm on the Q bands. These prove that multiple absorbing species are generated during the hetero-trimer formation process.

After calculations, based on the quantities of the two porphyrins involved in the reaction, a molar ratio resulting in TSPP/Pt-allyloxyPP = 2/1 and a structure were proposed, consisting of two TSPP molecules linked via oxygen atoms axially to the platinum atom in the Pt-allyloxyPP molecule, as presented in Figure 2c.

3.2. Characterization of the Pt-allyloxyPP-TSPP Hetero-Trimer

3.2.1. $^1\text{H-NMR}$ Analysis

In the $^1\text{H-NMR}$ spectrum recorded for the Pt-allyloxyPP-TSPP hetero-trimer (Figure S6), all the signals that support the formation of the hetero-trimer were found.

It is known that protons inside (in the centre) or above the porphyrin ring are in the shielding region, while the protons placed in the porphyrin plane periphery are in the deshielding region of the ring current effect [44].

Of major importance for the NMR spectra of the porphyrin dimers is the ring current effect and the intermolecular shielding generated by diamagnetic interactions with the other porphyrin neighbouring molecules. The presence in the vicinity of such large delocalized aromatic systems, together with their spatial orientation and distance toward the investigated core, might induce shielding or deshielding contributions [45]. So, this is the explanation of why the inner protons in NH- of TSPP free-base porphyrins resonate downfield to values of approximately -0.55 ppm, instead of the normal expected value of -2.7 ppm, and the pyrrole *meso* protons in the trimer structure resonate to upfield values of approximately 8.2 ppm, instead of 8.9 – 9.3 , as normal [46,47]. Thus, the internal protons of the TSPP molecules resonate at -0.55 ppm, due to the formation of a nonplanar structure, also favouring the supra-molecular assemblies [48] determining the diminution of the current cycle, so that the NH protons are less shielded [49–51]. The signal at 3.21 ppm is generated by the eight $-O-CH_2-CH=CH_2$ protons from the Pt-allyloxyPP porphyrin. The other protons in the group are identifiable as follows: the eight protons in the $=CH_2-$ group resonate as double doublet in the 4.15 – 4.22 ppm and 4.38 – 4.43 ppm domains, respectively; the four $-O-CH_2-CH=CH_2$ protons give a doublet signal in the 4.73 – 4.86 ppm range. The protons belonging to the phenyl group of Pt-allyloxyPP can be identified: *ortho* as a singlet at 6.35 ppm and *para* as a triplet centred at 6.63 ppm. The signals produced by the *ortho* protons belonging to the phenyl groups of TSPP are found as a multiplet at 7.07 ppm, and the ones in the *para*-position as multiplet at 7.36 ppm. The β -pyrrolic protons of the metallated porphyrin resonate in a much lower field than the doublet at 8.11 – 8.15 ppm (8.7 ppm in the bare metalloporphyrin [30]), because they are less deshielded by the applied magnetic field, due to the presence of the two enveloping TSPP molecules. In the case of the β -pyrrolic protons belonging to the tetrasulfonated porphyrins, they resonate as a doublet in the 8.25 – 8.28 ppm interval, as confirmed by the literature [34].

3.2.2. FT-IR Characterization

The infrared spectrum of TSPP (Figure 4) presents a band at 698 cm^{-1} , associated with the bending vibrations of the C–C bonds of the aromatic ring, that are overlapped with the C–S stretching vibration [39,52]. The band at 1023 cm^{-1} is attributed to S–O stretching vibration [34]. The symmetric stretching vibrations of SO_2 are present in the range 1438 – 1480 cm^{-1} [41]. The band at 1599 cm^{-1} is assigned to C–N stretching frequencies, which are overlapped with the C=C stretching of the phenyl ring [34].

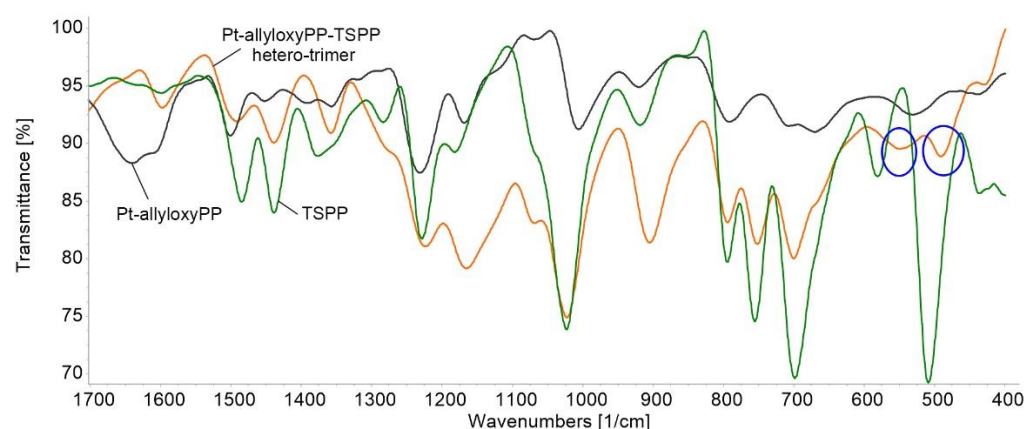


Figure 4. Overlapped FT-IR spectra for TSPP, Pt-allyloxyPP, and the Pt-allyloxyPP-TSPP hetero-trimer, as KBr pellets. The new generated bonds are marked in blue circles.

The FT-IR spectrum of Pt-allyloxyPP, together with its complete physical–chemical characterization, was presented in our previously published paper [30].

The FT-IR spectrum of Pt-allyloxyPP-TSPP hetero-trimer (Figure 4) presents features that are common to the starting porphyrins, with the exception of the new peaks located at

490 cm^{-1} and 549.5 cm^{-1} (blue circles in Figure 4) representing the bending vibration of Pt–O bond and confirming the proposed structure of the trimer [53].

3.3. Fluorimetric Detection of Toluidine Blue by the Pt-allyloxyPP-TSPP Hetero-Trimer

A solution of Pt-allyloxyPP-TSPP hetero-trimer in DMSO, having a concentration of 3.56×10^{-6} M, was acidulated to pH = 2, with HCl solution 37%. The UV–Vis absorption maximum of the Pt-allyloxyPP-TSPP hetero-trimer in the acidified solution is situated at 430 nm, due to formation of aggregated J-type species caused by protonation.

To 5 mL of this acidulated hetero-trimer solution, different volumes of toluidine blue solution in DMSO ($c = 1 \times 10^{-3}$ M) were added step-by-step. The obtained mixtures were stirred for 90 s, and the emission spectra were recorded and finally overlapped (Figure 5).

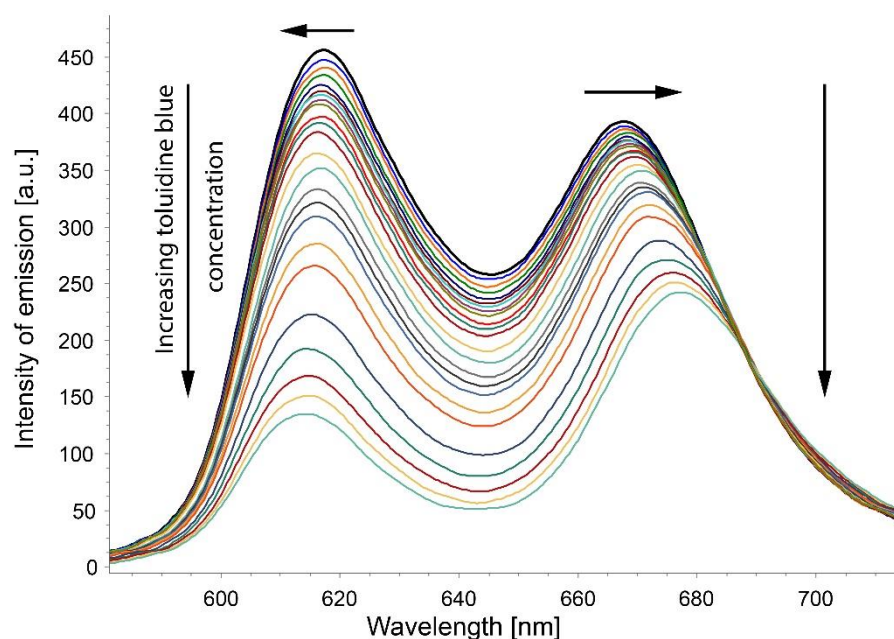


Figure 5. Emission spectra recorded during adding of toluidine blue to the acidified (pH = 2) solution of Pt-allyloxyPP-TSPP hetero-trimer in DMSO.

It can be observed that the adding of toluidine blue to the hetero-trimer solution produced changes, regarding both the wavelength location and the intensity of the fluorescence spectra. Thus, the peak located at 617 nm in the emission spectrum of the initial hetero-trimer was blue-shifted to 614 nm after exposure to TB, and the second peak, located initially at 668 nm, was bathochromically shifted with the increase in TB concentration to 677 nm. For obtaining the calibration curve, three experiments were performed, and the average intensity values were calculated. A constant fluorescence quenching accompanying the increase of toluidine blue concentration was also noticed. The decrease of intensity was more pronounced on the 617 nm band. The dependence of the intensity of emission and the toluidine blue concentration in the 1.9×10^{-6} – 6.39×10^{-5} M interval was linear (Figure 6), with a very good correlation coefficient of 99.59%. This domain is relevant for biological testing, because concentrations of TB higher than 50×10^{-6} M produce undesired DNA mutations [25–27,54].

A significant color modification of the Pt-allyloxy-TSPP hetero-trimer solution, from yellow to greenish blue, was observed, as illustrated before and after exposure to TB in visible (Figure 7a) and, respectively, under ultraviolet excitation (Figure 7b).

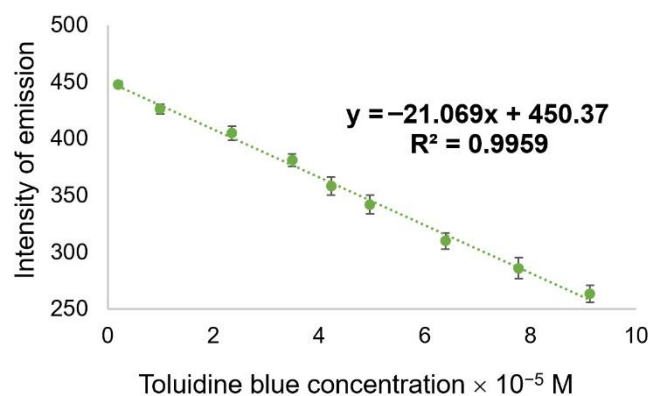


Figure 6. The linear dependence between the intensity of emission measured at 617 nm of the heterotrimer in DMSO (pH = 2) and the toluidine blue concentration, in the 1.9×10^{-6} – 6.39×10^{-5} M concentration range.



Figure 7. Photographic images of the Pt-allyloxy-TSPP trimer before and after exposure to TB, (a) in visible light and (b) under ultraviolet irradiation at 254 nm.

The fluorimetric detection of toluidine blue, presented in this work, has a limit of detection (LOD) of 1.4 μ M. The formula used to obtain the limit of detection [55–57] is presented as Equation (1):

$$\text{LOD} = 3\sigma/K \quad (1)$$

where σ is the standard deviation of blank measurement and K is the slope between the fluorescence versus analyte concentration.

Interference Test for Fluorimetric Detection of Toluidine Blue Using as Sensitive Material Pt-allyloxyPP-TSPP Hetero-Trimer

The interference study was performed on the following species that are neighbouring the tumour cells in the human body: sodium salicylate (SS), sodium acetate (SA), calcium gluconate (CaGlu), potassium iodide (KI), potassium chloride (KCl), ammonium oxalate (AmOxa), glucose (Glu), NaCl, urea, ascorbic acid (AA), and iron chloride (FeCl_3). The blank sample (Ref) consisted of 3 mL acidulated hetero-trimer solution in DMSO ($c = 3.56 \times 10^{-6}$ M), treated with 0.02 mL toluidine blue solution in water and 0.02 mL bi-distilled water, in order to have the same final concentration of TB in all samples tested ($c = 8.8 \times 10^{-5}$ M) and to disregard dilution effects. Each interference compound was added as a 0.02 mL solution in prepared concentrations, as to exceed the TB concentration by 100-fold. The emission spectra were overlapped and are presented in Figure S7, in the Supplementary File. The average percentage error was calculated according to the formula: $|\Delta I/I| \times 100$ [%], where I represents the emission intensity of the TB control sample (Ref), and ΔI is the difference between I and the emission intensity of the samples containing each studied interfering compound. It can be concluded that almost all of the compounds tested as interference compounds in the detection of TB (read at 617 nm) produced less than 1.5% average percentage error, as can be seen from Figure 8.

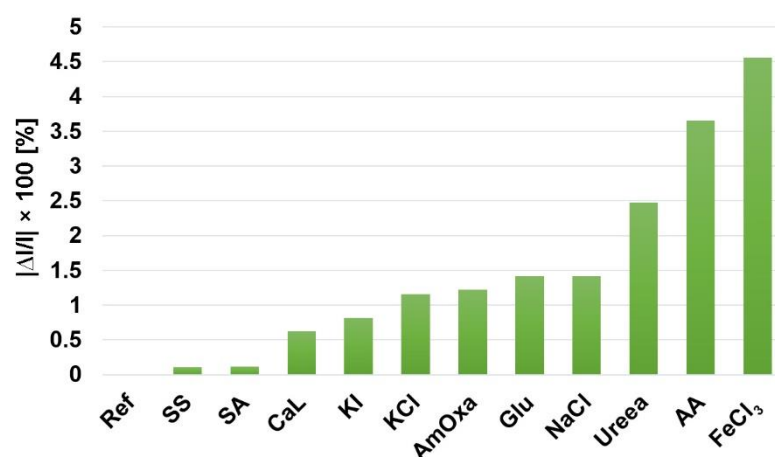


Figure 8. Average percentage error representation for the influence of several interference compounds (in concentrations exceeding 100 times the TB concentration), read at 617 nm.

3.4. AFM Investigations

The compared morphological aspects in the starting materials, in the porphyrin heterotrimer, and after the detection of toluidine blue, put into evidence after performing AFM microscopy, are presented in Figure 9.

The UV–Vis spectra changes convinced us that aggregation phenomena occurred during our investigations. It was also observed [48] that, if the ring current induced unexpected ¹H-NMR shifts, these are indicative of aggregate formation and, thus, these structures are well-suited to microscopy study. While in metalloporphyrins the central metal ion exerts a major role in aggregate generation, in the free base porphyrins, the weak π – π interactions, together with interactions involving peripheral substituents, influence the supramolecular organization.

In the case of Pt(II)-allyloxyPP (Figure 9a,b), triangular particles with dimensions in the 112.4–123.4 nm range, unevenly distributed, but having the same orientation, formed ring-type aggregates with large diameters between 557 nm and 1184 nm by helicoidal aggregation [58,59].

The deposition of TSPP from water (Figure 9c,d) leads to the formation of a porous surface, due to spherical particles, with diameters tailored in the 150 nm range.

The AFM images of Pt-allyloxyPP-TSPP heterotrimer (Figure 9e,f) displayed haystack-like formations produced by H-type aggregation of building-block particles that are extremely different architectures than those presented in the starting materials. The large aggregates distribution is uneven. The literature mentioned more structured prismatic geometries that are generated by multicomponent self-assembly, wherein two unique donor precursors are combined with a single Pt(II)-porphyrin acceptor [60].

After interaction with toluidine blue (Figure 9g,h), particles with higher dimensions, around 160–190 nm, that are more compactly distributed on the surface and having the tendency to gain together (Figure 9h), can be noticed. The H-type combined with J-type aggregations are more pronounced than in the absence of toluidine blue. The shape of the aggregates changed from haystacks, in the absence of TB, to ovoid droplets after the heterotrimer was exposed to TB.

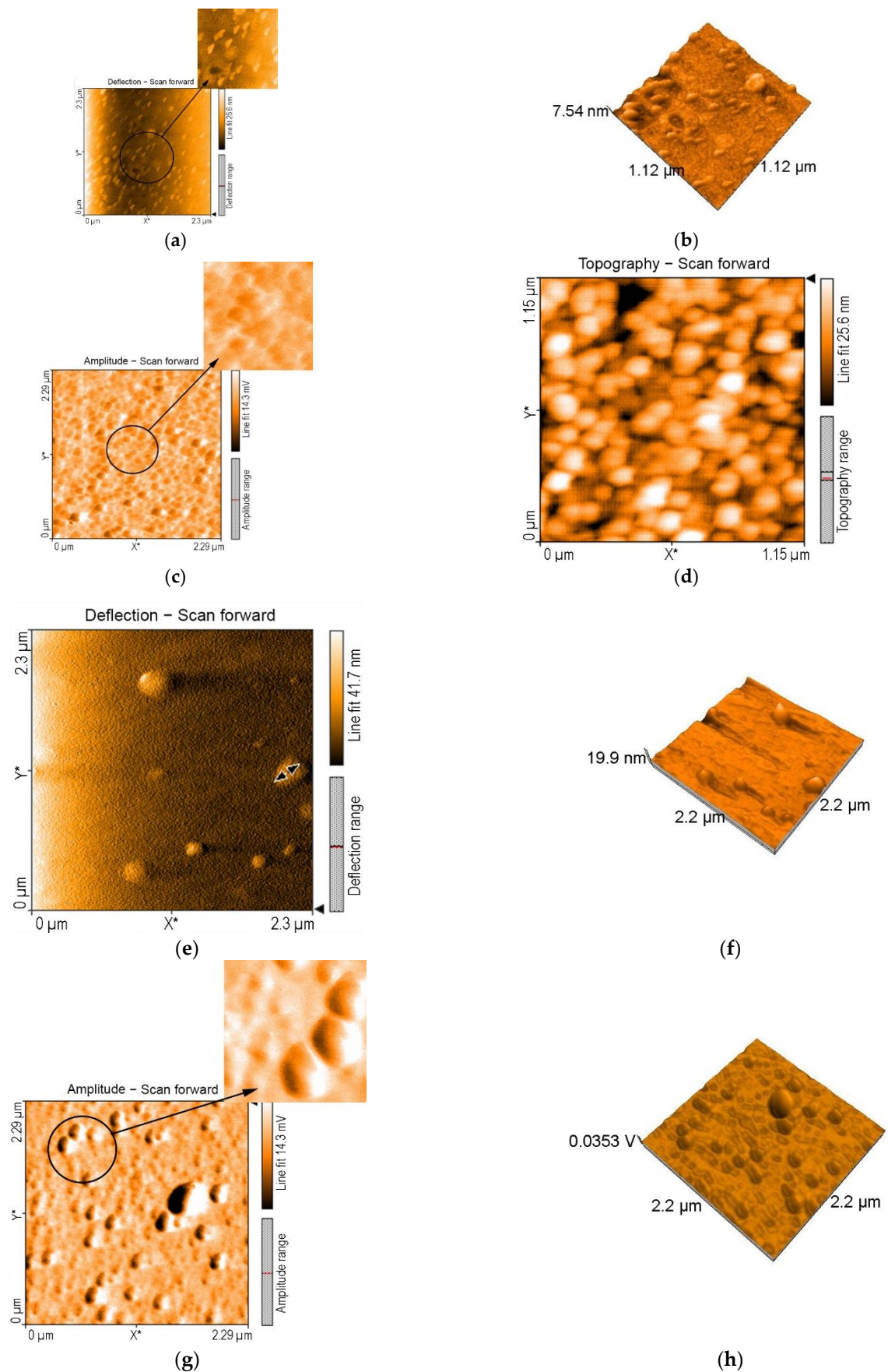


Figure 9. Atomic force microscopy images of (a,b) Pt-allyloxyPP, (c,d) TSPP, (e,f) Pt-allyloxyPP-TSPP hetero-trimer and (g,h) the complex after recognition of toluidine blue.

3.5. Infrared Spectra Comparison before and after the Detection of Toluidine Blue

The FT-IR spectrum of toluidine blue (Figure S8) presented all the bands corresponding to characteristic bonds. Thus, the C–N stretching frequency in the region $1381\text{--}1321\text{ cm}^{-1}$ and the C–N in-plane bending vibrations were identified at 663 cm^{-1} [61]. The band located at 698 cm^{-1} was assigned to C–S stretching vibration [62]. The bands around $1438\text{--}1480\text{ cm}^{-1}$ corresponded to vibrations of the C–H bonds [63]. The conjugated double bonds stretching vibration was evidenced at 1599 cm^{-1} [64].

The spectrum of the trimer after interaction with toluidine blue (Figure 10) presented all the common features of the initial materials and, in addition, the bands located at 1358 cm^{-1} and 1509 cm^{-1} , representing the vibration of the newly formed N–O bond between the positively charged nitrogen atom belonging to TB and the negatively charged oxygen atom corresponding to the SO_3 group [65]. The inter-molecular hydrogen bonding evidenced in the hetero-trimer at 3723 cm^{-1} [66,67] was no longer visible in the complex with TB, proving that the trimer molecules were involved in bonding with toluidine blue molecules and there were less sites available for hydrogen bonding.

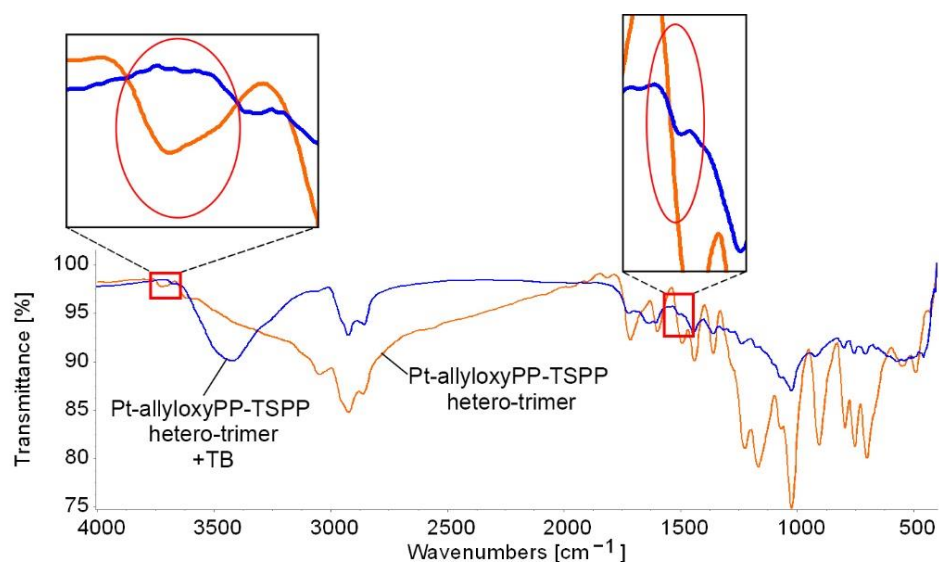


Figure 10. FT-IR spectra for Pt-allyloxyPP-TSPP hetero-trimer and the hetero-trimer after TB recognition.

The proposed mechanism for TB detection, using the hetero-trimer as a sensitive material, based on the spectroscopic and morphologic evidence and also as suggested by the program PyMOL molecular graphics system, due to suitable distances and spatial geometries, is a complex one, as presented in Figure 11. The three main interactions are simultaneously possible, as follows: positively charged nitrogen atoms from the TB molecules are linked to negatively charged oxygen atoms in the TSPP molecules by Coulombian forces (Figure 11, orange bonds); hydrogen bonds are generated between H atoms from amino groups and oxygen from sulfonic groups (Figure 11, green bonds); and $\pi\text{--}\pi$ interactions between sulphur from TB and one pyrrolic ring from porphyrins (Figure 11, yellow bonds).

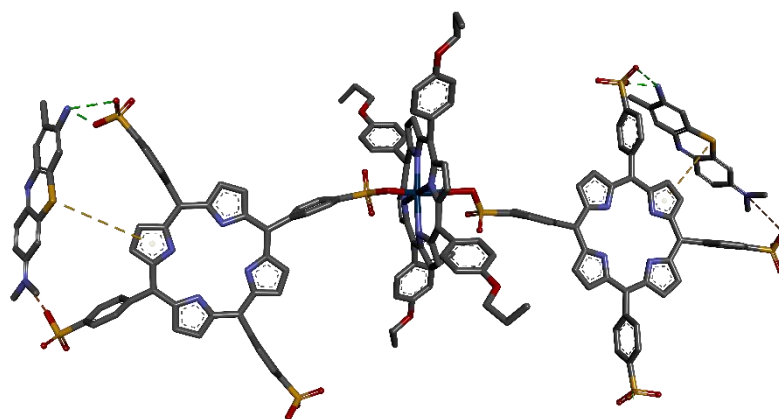


Figure 11. The proposed mechanism for TB detection using the hetero-trimer as sensitive material. Atom color coding follows standard CPK rules: carbon-black, oxygen-red, nitrogen-blue, sulfur-yellow, platinum-dark blue, hydrogen-white.

4. Conclusions

The formation of a porphyrin trimer, by the combination of a metallated porphyrin, Pt(II)-5,10,15,20-tetrakis-(4-allyloxyphenyl)-porphyrin (Pt-allyloxyPP), and a water-soluble porphyrin, 5,10,15,20-tetrakis(4-sulfonatophenyl)-porphyrin (TSPP), is presented. The hetero-trimer was characterized by UV-Vis, FT-IR, and $^1\text{H-NMR}$ spectroscopy, and the proposed structure was confirmed, consisting of two TSPP molecules linked to the platinum atom in the Pt-allyloxyPP molecule via oxygen atoms. This fluorescent hetero-trimer is able to detect toluidine blue in the biologically relevant concentration domain of 1.9×10^{-6} – 6.39×10^{-5} M, with a very good correlation coefficient of 99.59% for the linear dependence. The new porphyrin hetero-trimer offers the advantages of enhanced fluorescence properties and the presence of multiple acidic binding sites, favourable for the detection of toluidine blue. The morphology of the compared starting and synthesized materials, as revealed by AFM investigations, presents obvious differences. The hetero-trimer presents a haystack-like architecture of particles, unevenly distributed on the surface, whereas, after exposure to toluidine blue, the surface is more evenly covered with the drop-like ovoid aggregates obtained by the amplification of both J- and H-type aggregation.

This work brings attention to the first fluorescent sensor for toluidine blue, purposely designed for testing medical concentrations, as it is known that an excess of 50 μM TB in culture cells is carcinogenic.

Supplementary Materials: The following supporting information can be downloaded at: <https://www.mdpi.com/article/10.3390/chemosensors10110481/s1>, Table S1. Porphyrins used for the formation of homo- and hetero-dimers and trimers, with or without linkers and their applications; Figure S1. UV-Vis spectrum of 5,10,15,20-tetrakis(4-sulfonatophenyl)-porphyrin (TSPP) in ethanol ($c = 6.4377 \times 10^{-6}$ M); Figure S2. UV-Vis spectra for TSPP ($c = 8 \times 10^{-6}$ M) at initial pH = 4.9 and at acid pH = 1.4 for the same concentration; Figure S3. The emission spectra of TSPP at different pH values; Figure S4. FT-IR spectrum of 5,10,15,20-tetrakis(4-sulfonatophenyl)-porphyrin (TSPP); Figure S5. Overlapped UV-Vis spectra during the formation of the hetero-trimer. In detail, the Q bands; Figure S6. $^1\text{H-NMR}$ spectrum of the Pt-allyloxyPP-TSPP hetero-trimer; Figure S7. Overlapped emission spectra for interfering species that are exceeding 100 times the concentration of the main analyte (toluidine blue, represented as Ref curve); Figure S8. FT-IR spectrum of toluidine blue.

Author Contributions: Conceptualization, E.F.-C.; methodology, E.F.-C. and M.B.; software, I.F. and M.B.; validation, E.F.-C.; formal analysis, A.L., C.E., I.F., L.H. and M.B.; investigation, A.L., C.E., I.F. and M.B.; resources, E.F.-C.; data curation, A.L., I.F. and L.H.; writing—original draft preparation, A.L., I.F. and E.F.-C.; writing—review and editing, E.F.-C.; visualization, I.F. and E.F.-C.; supervision, E.F.-C.; project administration, E.F.-C.; funding acquisition, E.F.-C. All authors have read and agreed to the published version of the manuscript.

Funding: This research was funded by Romanian Academy, through program 3/2022 from the Institute of Chemistry “Coriolan Dragulescu”, and by UEFISCDI, grant number 76 PCCDI/2018-ECOTECH-GMP.

Institutional Review Board Statement: Not applicable.

Informed Consent Statement: Not applicable.

Data Availability Statement: The data presented in this study are available on request from the corresponding author.

Conflicts of Interest: All authors declare that the research was conducted in the absence of any commercial or financial relationships that could be construed as a potential conflict of interest.

References

1. Nomoto, A.; Mitsuoka, H.; Ozeki, H.; Kobuke, Y. Porphyrin hetero-dimer as charge separating system for photocurrent generation. *Chem. Commun.* **2003**, *9*, 1074–1075. [CrossRef]
2. Liu, Y.; Lin, H.; Li, J.; Dy, J.T.; Tamaki, K.; Nakazaki, J.; Nakayama, D.; Nishiyama, C.; Uchida, S.; Kubo, T.; et al. Ethynyl-linked push–pull porphyrin hetero-dimers for near-IR dye-sensitized solar cells: Photovoltaic performances versus excited-state dynamics. *Phys. Chem. Chem. Phys.* **2012**, *14*, 16703. [CrossRef]
3. Mazur, L.M.; Roland, T.J.; Leroy-Lhez, S.; Sol, V.; Samoc, M.; Samuel, I.D.W.; Matczyszyn, K. Efficient Singlet Oxygen Photogeneration by Zinc Porphyrin-Dimers Upon One- and Two-Photon Excitation. *J. Phys. Chem. B* **2019**, *123*, 4271–4277. [CrossRef]
4. Li, Q.; Li, C.; Baryshnikov, G.; Ding, Y.; Zhao, C.; Gu, T.; Sha, F.; Liang, X.; Zhu, W.; Wu, X.; et al. Twisted-Planar-Twisted expanded porphyrinoid dimer as a rudimentary reaction-based methanol indicator. *Nat. Commun.* **2020**, *11*, 5289. [CrossRef]
5. Fagadar-Cosma, E.; Badea, V.; Fagadar-Cosma, G.; Palade, A.; Lascu, A.; Fringu, I.; Birdeanu, M. Trace oxygen sensitive material based on two porphyrin derivatives heterodimer complex. *Molecules* **2017**, *22*, 1787. [CrossRef]
6. Manera, M.G.; Ferreira-Vila, E.; García-Martín, J.M.; Cebollada, A.; García-Martín, A.; Giancane, G.; Valli, L.; Rella, R. Enhanced magneto-optical SPR platform for amine sensing based on Zn porphyrin dimers. *Sens. Actuators B Chem.* **2013**, *182*, 232–238. [CrossRef]
7. Schmitt, J.; Jenni, S.; Sour, A.; Heitz, V.; Bolze, F.; Pallier, A.; Bonnet, C.; Toth, E.; Ventura, V. A Porphyrin Dimer–GdDOTA Conjugate as a Theranostic Agent for One- and Two-Photon Photodynamic Therapy and MRI. *Am. Chem. Soc.* **2018**, *29*, 3726–3738. [CrossRef]
8. Chiang, Y.H.; Chou, H.H.; Cheng, W.T.; Li, Y.R.; Yeh, C.Y.; Chen, P. Porphyrin dimers as hole-transporting layers for high-efficiency and stable perovskite solar cells. *ACS Energy Lett.* **2018**, *3*, 1620–1626. [CrossRef]
9. Vysniauskas, A.; Ding, D.; Qurashi, M.; Boczarow, I.; Balaz, M.; Anderson, H.; Kuimova, M. Tuning the sensitivity of fluorescent porphyrin dimers to viscosity and temperature. *Chem.-Eur. J.* **2017**, *23*, 11001–11010. [CrossRef]
10. Lamare, R.; Ruppert, R.; Elhabiri, M.; Ulrich, G.; Ruhlmann, L.; Weiss, J. Design and Synthesis of Charged Porphyrin Dimers for Polyoxometalate Recognition. *C. R. Chim.* **2021**, *24*, pp. 115–126. Available online: <https://comptes-rendus.academie-sciences.fr/chimie/articles/10.5802/crchim.105/> (accessed on 8 November 2022).
11. Habets, T.; Lensen, D.; Speller, S.; Elemans, J.A. Self-assembly of covalently linked porphyrin dimers at the solid–liquid interface. *Molecules* **2019**, *24*, 3018. [CrossRef]
12. Schissler, C.; Schneider, E.K.; Felker, B.; Weis, P.; Nieger, M.; Kappes, M.M.; Bräse, S. A Synthetic Strategy for Cofacial Porphyrin-Based Homo- and Heterobimetallic Complexes. *Chem.-Eur. J.* **2021**, *27*, 3047–3054. [CrossRef]
13. Gil-Ramírez, G.; Karlen, S.D.; Shundo, A.; Porfyrakis, K.; Ito, Y.; Briggs, G.A.D.; Morton, J.J.L.; Anderson, H.L. A Cyclic Porphyrin Trimer as a Receptor for Fullerenes. *Org. Lett.* **2010**, *12*, 3544–3547. [CrossRef]
14. Fang, X.; Zhou, Y.-Z.; Zheng, J.-Y. Clawlike Tripodal Porphyrin Trimer: Ion-Controlled On–Off Fullerene Binding. *J. Org. Chem.* **2014**, *79*, 1184–1191. [CrossRef]
15. Kato, K.; Osuka, A. Propeller-shaped Semi-fused Porphyrin Trimers: Molecular symmetry-dependent Chiroptical Response. *Chem. Eur. J.* **2020**, *26*, 10217–10221. [CrossRef]
16. Tyurin, V.S.; Mikhalitsyna, E.A.; Semeikin, A.S.; Beletskaya, I.P. Synthesis of New Porphyrin Trimers via Buchwald-Hartwig Amination Reaction. *Macromolecules* **2015**, *8*, 358–365. [CrossRef]
17. Polevaya, Y.P.; Tyurin, V.S.; Beletskaya, I.P. Linear conjugated porphyrin trimer synthesis via “click” reaction. *J. Porphyr. Phthalocyanines* **2013**, *17*, 1–15. [CrossRef]
18. Hamamura, T.; Nakazaki, J.; Uchida, S.; Kubo, T.; Segawa, H. Controlling the Rotation of Porphyrin Units in Ethynyl-linked Porphyrin Trimers for Dye-sensitized Solar Cells by Anchoring onto TiO₂ Surface. *Chem. Lett.* **2014**, *43*, 796–798. [CrossRef]
19. Bhuse, D.V.; Bhuse, V.M.; Bhagat, P.R. Star-type melamine based conjugated carboxy functionalized porphyrin trimer for DSSCs: An efficient approach to clean, aggregation free and true energy generation. *Mater. Chem. Phys.* **2022**, *287*, 126312. [CrossRef]
20. Sridharan, G.; Shankar, A.A. Toluidine blue: A review of its chemistry and clinical utility. *J. Oral Maxillofac. Pathol.* **2012**, *16*, 251–255. [CrossRef]

21. Singh, S.; Halder, A.; Sinha, O.; Chakrabarty, N.; Chatterjee, T.; Adhikari, A.; Singh, P.; Shikha, D.; Ghosh, R.; Banerjee, A.; et al. Spectroscopic Studies on the Biomolecular Recognition of Toluidine Blue: Key Information Towards Development of a Non-Contact, Non-Invasive Device for Oral Cancer Detection. *Front. Oncol.* **2020**, *10*, 529132. [[CrossRef](#)]
22. Mills, S. How effective is toluidine blue for screening and diagnosis of oral cancer and premalignant lesions? *Evid. Based Dent.* **2022**, *23*, 34–35. [[CrossRef](#)]
23. Raja, N.; Naikodi, S.; Govindarajan, A.; Palanisamy, K. Toluidine blue staining of murine mast cells and quantitation by a novel, automated image analysis method using whole slide skin images. *J. Histotechnol.* **2021**, *44*, 190–195. [[CrossRef](#)]
24. Wong, A.L.; Hricz, N.; Malapati, H.; von Guionneau, N.; Wong, M.; Harris, T.; Boudreau, M.; Cohen-Adad, J.; Tuffaha, S. A simple and robust method for automating analysis of naïve and regenerating peripheral nerves. *PLoS ONE* **2021**, *16*, e0248323. [[CrossRef](#)]
25. Redman, R.S.; Krasnow, S.H.; Sniffen, R.A. Evaluation of the carcinogenic potential of toluidine blue O in the hamster cheek pouch. *Oral Surg. Oral Med. Oral Pathol.* **1992**, *74*, 473–480. [[CrossRef](#)]
26. Dunipace, A.J.; Beaven, R.; Noblitt, T.; Yiming, L.; Zunt, S.; Stookey, G. Mutagenic potential of toluidine blue evaluated in the Ames test. *Mutat Res.* **1992**, *279*, 255–259. [[CrossRef](#)]
27. Bekka, E.; Hopfer, C.; Eyer, F.; Muckter, H.; Gudermann, T. Mitochondrial toxicity and oxidative stress induced by methylene blue and toluidine blue in mammalian cells. *Clin. Toxicol.* **2018**, *56*, 453–608. [[CrossRef](#)]
28. Ali, F.F. Adsorption of Toluidine blue dye from industrial waste water on the remnants of tea leaf. *Int. J. Chemtech. Res.* **2017**, *10*, 497–507.
29. Dudas, Z.; Enache, C.; Fagadar-Cosma, G.; Armeanu, I.; Fagadar-Cosma, E. Hybrid silica-porphyrin materials with tailored pore sizes. *Mater. Res. Bull.* **2010**, *45*, 1150–1156. [[CrossRef](#)]
30. Fagadar-Cosma, E.; Plesu, N.; Lascu, A.; Anghel, D.; Cazacu, M.; Ianasi, C.; Fagadar-Cosma, G.; Fratilescu, I.; Epuran, C. Novel Platinum-Porphyrin as Sensing Compound for Efficient Fluorescent and Electrochemical Detection of H₂O₂. *Chemosensors* **2020**, *8*, 29. [[CrossRef](#)]
31. Song, R.; Robert, A.; Bernadou, J.; Meunier, B. Sulfonated and acetamidodisulfonated tetraarylporphyrins as biomimetic oxidation catalysts under aqueous conditions. *Inorg. Chim. Acta* **1998**, *272*, 228–234. [[CrossRef](#)]
32. Busby, C.; DiNello, R.K.; Dolphin, D. A Convenient Preparation of meso-Tetra(4-sulfonatophenyl)porphyrin. *Can. J. Chem.* **1975**, *55*, 1554–1555. [[CrossRef](#)]
33. Hambright, P. Chemistry of water soluble porphyrins. In *The Porphyrin Handbook*; Kadish, K.M., Smith, K.M., Guillard, R., Eds.; Academic Press: San Diego, CA, USA, 2000; pp. 129–210.
34. Tsolekile, N.; Ncapayi, V.; Obiyanwa, G.K.; Songca, S.; Oluwafemi, O.S. Synthesis of meso-tetra-(4-sulfonatophenyl) porphyrin (TPPS4)—CuInS/ZnS quantum dots conjugate as an improved photosensitizer. *Int. J. Nanomed.* **2019**, *14*, 7065–7078. [[CrossRef](#)]
35. Sobczynski, J.; Tonnesen, H.H.; Kristensen, S. Influence of aqueous media properties on aggregation and solubility of four structurally related meso-porphyrin photosensitizers evaluated by spectrophotometric measurements. *Pharmazie* **2013**, *68*, 100–109. [[CrossRef](#)]
36. Zhao, L.; Liu, M.; Li, A.; An, H.; Ye, H.; Zhang, Y. Aggregation and supramolecular chirality of 5,10,15,20-tetrakis-(4-sulfonatophenyl)-porphyrin on achiral poly(2-(dimethylamino)ethyl methacrylate)-grafted ethylene-vinyl alcohol membrane. *J. Mater. Chem. C* **2015**, *3*, 3650–3658. [[CrossRef](#)]
37. Wurthner, F.; Keiser, T.E.; Saha-Moller, C.R. J-Aggregates: From Serendipitous Discovery to Supramolecular Engineering of Functional Dye Materials. *Angew. Chem. Int. Ed.* **2011**, *50*, 3376–3410. [[CrossRef](#)]
38. Hanyz, I.; Wrobel, D. The influence of pH on charged porphyrins studied by fluorescence and photoacoustic spectroscopy. *Photochem. Photobiol. Sci.* **2002**, *1*, 126–132. [[CrossRef](#)]
39. Marcioni, M.; Alongi, J.; Ranucci, E.; Malinconico, M.; Laurienzo, P.; Ferruti, P.; Manfredi, A. Semi-Crystalline Hydrophobic Polyamidoamines: A New Family of Technological Materials? *Polymers* **2021**, *13*, 1018. [[CrossRef](#)]
40. Kathiravan, A.; Kumar, P.S.; Renganathan, R.; Anandan, S. Photoinduced electron transfer reactions between meso-tetrakis(4-sulfonatophenyl)porphyrin and colloidal metal-semiconductor nanoparticles *Colloids Surf. A Physicochem. Eng. Asp.* **2009**, *333*, 175–181. [[CrossRef](#)]
41. Anto, P.L.; Anto, R.J.; Varghese, H.T.; Panicker, C.Y.; Philipe, D.; Brolo, A.G. FT-IR, FT-Raman and SERS spectra of anilinium sulfate. *J. Raman Spectrosc.* **2009**, *40*, 1810–1815. [[CrossRef](#)]
42. Fagadar-Cosma, E.; Vlascici, D.; Birdeanu, M.; Fagadar-Cosma, G. Novel fluorescent pH sensor based on 5-(4-carboxyphenyl)-10,15,20-tris(phenyl)-porphyrin. *Arab. J. Chem.* **2019**, *12*, 1587–1594. [[CrossRef](#)]
43. Fagadar-Cosma, E.; Enache, C.; Tudose, R.; Armeanu, I.; Mosoarca, E.; Vlascici, D.; Costisor, O. UV-VIS and Fluorescence Spectra of Meso-Tetraphenylporphyrin and Meso-Tetrakis-(4-Metoxypheyl) Porphyrin in the THF and THF Water Systems The influence of pH. *Rev. Chim. Buc.* **2007**, *58*, 451–455.
44. Gjuroski, I.; Furrer, J.; Vermathen, M. Probing the Interactions of Porphyrins with Macromolecules Using NMR Spectroscopy Techniques. *Molecules* **2021**, *26*, 1942. [[CrossRef](#)]
45. Pretsch, E.; Clerc, T.; Seibl, J.; Simon, W. Protonenresonanzspektroskopie. In *Tabellen zur Strukturaufklärung Organischer Verbindungen Mit Spektroskopischen Methoden*; Fresenius, W., Huber, J.F.K., Pungor, E., Rechnitz, G.A., Tölg, G., West, T.S., Eds.; Springer: Berlin/Heidelberg, Germany, 1981; Volume 15, pp. 108–181.
46. Hunter, C.A.; Sanders, J.K.M. The nature of pi-pi interactions. *J. Am. Chem. Soc.* **1990**, *112*, 5525–5534. [[CrossRef](#)]

47. Abraham, R.J.; Smith, K.M. NMR spectra of porphyrins. 21. Applications of the ring-current model to porphyrin and chlorophyll aggregation. *J. Am. Chem. Soc.* **1983**, *105*, 5734–5741. [[CrossRef](#)]
48. Vermathen, M.; Marzorati, M.; Bigler, P. Self-Assembling Properties of Porphyrinic Photosensitizers and Their Effect on Membrane Interactions Probed by NMR Spectroscopy. *J. Phys. Chem. B* **2013**, *117*, 6990–7001. [[CrossRef](#)]
49. Ryan, A.; Gehrold, A.; Perusitti, R.; Pintea, M.; Fazekas, M.; Locos, O.B.; Blaikie, F.; Senge, M.O. Porphyrin Dimers and Arrays. *Eur. J. Org.* **2011**, *29*, 5817–5844. [[CrossRef](#)]
50. Norvaiša, K.; O'Brien, J.E.; Gibbons, D.J.; Senge, M.O. Elucidating Atropisomerism in Nonplanar Porphyrins with Tunable Supramolecular Complexes. *Eur. J. Chem.* **2020**, *27*, 331–339. [[CrossRef](#)]
51. Webb, M.J.; Deroo, S.; Robinson, C.V.; Bampos, N. Host-guest interactions in acid-porphyrin complexes. *Chem. Commun.* **2012**, *48*, 9358–9360. [[CrossRef](#)]
52. Chandran, M.; Sankara, S.P.; Bhagatsingh, R.; Shunmuganarayanan, A.; Navaneethakrishnan, S.; Rajaputi, V. FT-IR and FT-Raman Spectroscopic Analyses of Indeno Quinoxaline Derivative Crystal. *Asian J. Appl. Sci.* **2018**, *11*, 83–91. [[CrossRef](#)]
53. Jones, J.R.; Hench, L.L. Biomedical materials, fourier transform infrared spectroscopy. In *Encyclopedia of Condensed Matter Physics*; Bassani, F., Liedl, G.L., Wyder, P., Eds.; Elsevier: Amsterdam, The Netherlands, 2005; pp. 108–116, ISBN 9780123694010. [[CrossRef](#)]
54. Yamasaki, H.; Komoto, S. Mechanism of Histamine Release by Toluidine Blue from Rat Mast Cells. *Int. Arch. Allergy Immunol.* **1971**, *41*, 854–867. [[CrossRef](#)]
55. Mei, Q.; Shi, Y.; Hua, Q.; Tong, B. Phosphorescent chemosensor for Hg²⁺ based on iridium(III) complex coordinated with 4-phenylquinazoline and sodium carbazole dithiocarbamate. *RSC Adv.* **2015**, *5*, 74924–74931. [[CrossRef](#)]
56. Long, G.L.; Winefordner, J.D. Limit of detection. A closer look at the IUPAC definition. *Anal. Chem.* **1983**, *55*, 712–724. [[CrossRef](#)]
57. Shrivastava, A.; Gupta, V.B. Methods for the determination of limit of detection and limit of quantitation of the analytical methods. *Chron. Young Sci.* **2011**, *2*, 21–25. [[CrossRef](#)]
58. Fagadar-Cosma, E.; Fagadar-Cosma, G.; Vasile, M.; Enache, C. Synthesis, Spectroscopic and Self-Assembling Characterization of Novel Photoactive Mixed Aryl-Substituted Porphyrin. *Curr. Org. Chem.* **2012**, *16*, 931–941. [[CrossRef](#)]
59. Tarabukina, E.; Fagadar-Cosma, E.; Enache, C.; Zakharova, N.; Birdeanu, M. Molecular Properties and Aggregation of Porphyrin Modified Polysiloxane in Solutions. *J. Macromol. Sci. B Phys.* **2013**, *52*, 1077–1091. [[CrossRef](#)]
60. Shi, Y.; Sanchez-Molina, I.; Cao, C.; Stang, P.J. Synthesis and photophysical studies of self-assembled multicomponent supramolecular coordination prisms bearing porphyrin faces. *Proc. Natl. Acad. Sci. USA* **2014**, *111*, 9390–9395. [[CrossRef](#)]
61. Balachandran, V.; Murali, M.K. FT-IR and FT-Raman spectral analysis of 3-(trifluoromethyl) phenyl isothiocyanate. *Elixir Vib. Spec.* **2011**, *40*, 5105–5107.
62. Muthuselvi, C.; Pandiarajan, S.S.; Ravikumar, B.; Athimoolam, S.; Krishnakumar, R.V. Spectroscopic Investigation of 7'-Nitro-6'-phenyl-1',6',7',7a'- tetrahydro-spiro[indeno[1,2-b]quinoxaline-11,5'-pyrrolo[1,2-c] [1,3]thiazole] Crystal. *Asian J. Appl. Sci.* **2018**, *11*, 9–19. [[CrossRef](#)]
63. Adar, F. FT-IR and Raman: A Synergism, Not Competing Technologies. *Spectroscopy* **2009**, *24*. Available online: <https://www.spectroscopyonline.com/view/ft-ir-and-raman-synergism-not-competing-technologies-0> (accessed on 14 November 2022).
64. Hadjamar, Z.; Chabira, S.f.; Sebaa, M. FTIR-ATR Analysis, Curve Fitting of Rigid PVC Tube Used in Industrial Areas. In Proceedings of the 2nd International Conference on Industry 4.0 and Artificial Intelligence (ICIAI 2021), Sousse, Tunisia, 28–30 November 2021. [[CrossRef](#)]
65. Kubicki, J.; Lorenc, M.; Cochelin, P.; Mongin, O.; Amar, A.; Boucekkine, A.; Gaje, A.; Humphrey, M.G.; Morshedi, M.; Lorenzen, S.; et al. Nitro End Groups Remarkable Vibrational Reporters for Charge Transfer in the Excited States of Oligo(p-phenyleneethynylene)- Bridged Donor-Acceptor Dyads. *J. Phys. Chem. C* **2020**, *124*, 9755–9764. [[CrossRef](#)]
66. Cichosz, S.; Masek, A. IR study on cellulose with the varied moisture contents: Insight into the supramolecular structure. *Materials* **2020**, *13*, 4573. [[CrossRef](#)]
67. Mora, A.S.; Tayouo, R.; Boutevin, B.; David, G.; Caillol, S. A perspective approach on the amine reactivity and the hydrogen bonds effect on epoxy-amine systems. *Eur. Polym. J.* **2020**, *123*, 109460. [[CrossRef](#)]